Petroleum Science 23 (2026) 514–523

Contents lists available at ScienceDirect

Petroleum Science

journal homepage: www.keaipublishing.com/en/journals/petroleum-science

Original Paper

Unveiling the role of residual structure in hydrate secondary formation through molecular dynamics simulations

Yi-Fan Zhang, Sen-Bo Xiao *, Zhi-Liang Zhang, Jian-Ying He **

NTNU Nanomechanical Lab, Department of Structural Engineering, Norwegian University of Science and Technology (NTNU), Trondheim, 7491, Norway

ARTICLE INFO

Article history:
Received 25 March 2025
Received in revised form
4 September 2025
Accepted 6 November 2025
Available online 12 November 2025

Edited by Teng Zhu

Keywords:
Natural gas hydrate
Secondary formation
Residual structure
Gas supersaturation
Flow assurance
Molecular dynamics

ABSTRACT

The rapid secondary formation of gas hydrate is a potential cause of flowline blockage in deepwater oil and gas production systems, posing serious flow assurance challenges. However, its microscopic formation mechanism remains an area of active research. Recently, the residual structure hypothesis has gained significant attention in explaining the rapid secondary formation of hydrates. In this study, massive molecular dynamics simulations are conducted to investigate the secondary formation of methane hydrates in solutions containing hydrate residual structures of varying sizes. The results indicated that residual structures, owing to their hydrate-like characteristics, facilitate the adsorption and capture of methane molecules, leading to the formation of local gas supersaturation regions. Residual structures promote hydrate formation through two key mechanisms: acting as nucleation sites and supplementing methane concentrations. Particularly, a synergy between residual structures and gas concentration was identified: high gas concentrations stabilize small residual structures, allowing them to serve as nucleation sites, while large stable structures can enrich methane even under low gas concentration.

This work not only provided a detailed understanding of the mechanisms of hydrate secondary formation but also provided valuable insight for hydrate blockage prediction and control in subsea oil and gas pipelines, contributing to improved flow assurance strategies.

1. Introduction

With the rapid development of technology and the economy, global energy demand continues to increase, and petroleum and natural gas remain the primary energy sources (Cook, 2021; Dyatlov et al., 2020; Haider, 2020). However, the exploitation of deep-sea oil, gas and hydrate resources faces numerous challenges, among which hydrate-induced pipeline blockage is the key issue that affects the safety and economic viability of subsea oil and gas transportation (Li et al., 2023; Wang et al., 2023a; Zhang et al., 2024a). Due to the high-pressure and low-temperature environment of deep-sea pipelines, natural gas hydrates can rapidly form and accumulate within the pipelines, leading to a decline in transportation capacity or even complete blockage, which may cause production interruptions and safety incidents (Zhang et al., 2024a, 2024b). To address the hydrate blockage issue, the industry has adopted several flow assurance strategies, including the injection of additives, pipeline heating, and mechanical removal (Shi et al., 2021; Wang et al., 2023a). However, these approaches have limitations, such as high costs, environmental impact, and operational challenges, making it difficult to fundamentally prevent hydrate formation and accumulation in pipelines. Therefore, a comprehensive understanding of the hydrate formation mechanism in subsea pipelines is essential for developing more efficient and sustainable mitigation strategies.

Gas hydrate is a crystalline structure in which water molecules form cage-like structures through hydrogen bonding, encapsulating gas molecules (such as methane, carbon dioxide, and hydrogen) as guest molecules in the cavities (Hassanpouryouzband et al., 2020). Gas hydrates are widely distributed in marine sediments and permafrost and are considered an alternative energy source with great potential, as one cubic meter of gas hydrate can store approximately 180 cubic meters of

* Corresponding author.
** Corresponding author.
E-mail addresses: senbo.xiao@ntnu.no (S.-B. Xiao), jianying.he@ntnu.no (J.-Y. He).

Peer review under the responsibility of China University of Petroleum (Beijing).

https://doi.org/10.1016/j.petsci.2025.11.017

carbon dioxide (Sadeh et al., 2024) or 164 cubic meters of methane (Sadeh et al., 2024). Based on the type and size of guest molecules, hydrate can be classified into Structure I (SI), Structure II (SII), and Structure H (SH) (Karaaslan et al., 2002), with SI methane hydrate being the primary type in the deep-sea transport pipeline dominated by methane-rich gas compositions (Ying et al., 2019). In recent years, significant progress has been made in gas hydrate research, leading to the accumulation of extensive theoretical and experimental data on hydrate formation behavior (Moon et al., 2003; You et al., 2019). Hydrate formation is constrained by both thermodynamic and kinetic factors, requiring high-pressure and low-temperature conditions (Sloan Jr and Koh, 2007). Studies have shown that the hydrate formation rate is determined by factors such as supercooling and gas mass transfer rates (Liang et al., 2022; Maeda et al., 2012). Moreover, the formation of hydrates involves a lengthy growth period due to a complex phase transition process (Kvamme et al., 2020). However, in actual pipeline environments, the observed hydrate formation rate is significantly faster than that reported in laboratory studies, exhibiting atypical kinetic characteristics (Mo et al., 2022; Sayani et al., 2020; Wang et al., 2020). This phenomenon indicates that the hydrate formation within the pipeline may involve more complex microscopic interaction mechanisms, such as oil-phase composition and the presence of impurities (Liu et al., 2022; Lv et al., 2024).

After decades of research, the phenomenon of hydrate secondary formation, first discovered in 1884 (Roozeboom, 1884), is considered one of the primary factors contributing to rapid hydrate formation in pipelines (Kim et al., 2020; Liu et al., 2021b; Seo and Kang, 2012). Strikingly, the rate of hydrate formation in a water-gas mixed system of freshly melted hydrate is generally orders of magnitude faster than in newly-prepared water-gas solutions (Chen et al., 2020; Wei and Maeda, 2023). Due to the low temperature, high pressure, and high gas concentration, hydrate can readily form within the transportation pipelines. The corresponding hydrate blockage phenomenon exhibits similar characteristics to secondary formation, such as rapid formation rate, short induction time. As a result, the shortened induction time in hydrate secondary formation has drawn significant attention in hydrate-related research relevant to pipeline flow assurance (Buchanan et al., 2005; Kou et al., 2022; Zheng et al., 2022), especially about flow assurance and hydrate blockage risks in subsea pipelines. Therefore, the mechanism underlying the secondary formation of hydrates remains a critical topic of investigation (Gao et al., 2023; Kou et al., 2022).

Owing to the extensive research conducted over the past few decades, three main hypotheses have been proposed to explain the secondary formation of hydrate: the gas supersaturation hypothesis (Bagherzadeh et al., 2013), the impurity imprinting hypothesis (Zeng et al., 2006), and the residual structure hypothesis (Wu and Zhang, 2010), each originating from a distinct perspective. The gas supersaturation hypothesis suggests that the nanobubbles formed after hydrate decomposition can enhance gas transfer, thereby promoting secondary formation. The impurity imprinting hypothesis proposes that hydrate preferentially form on impurity surfaces, leaving imprints that act as nucleation sites for secondary formation by lowering the energy barrier. Compared to the above two hypotheses, the residual structure hypothesis, which is the oldest one, continues to attract great interest. The residual structure hypothesis suggests that the major cause of hydrate secondary formation in freshly melted water-gas mixture is the presence of partially decomposed residual hydrate structures. These residual structures, exhibiting hydrate-like properties, serve as nucleation sites and significantly reduce the induction time of hydrate formation. Over the past decade, researchers have obtained crucial new insights into the residual structure hypothesis. Study has shown that the residual cup-cage structures with gas molecules can effectively promote hydrate formation (Cheng et al., 2024). In addition, the decomposition temperature and duration have been found to significantly affect the induction time of hydrate formation (Zheng et al., 2022). However, to fully understand the role of residual structures in secondary hydrate formation, many unresolved issues still need to be addressed. For example, the microscopic interactions between methane molecules and residual hydrate structures remain unclear. Additionally, how residual structures accelerate hydrate formation is still not fully understood at the molecular level. Previous studies have shown that the structural stability of hydrates is strongly influenced by gas concentration (Cheng et al., 2026; Wang et al., 2023b). In the presence of residual structures, the promotion mechanism of gas concentration on the hydrate secondary formation remains unclear. The potential synergistic effect between residual structures and gas concentration during secondary formation has not yet been explored. Addressing these unresolved questions is crucial for advancing the mechanisms of secondary formation of hydrate and its potential applications in improving flow assurance strategies in subsea oil and gas production.

Due to the small size of residual structure, investigating the microscopic mechanism of the residual structure hypothesis is generally beyond the resolution limits of length scale in traditional experiments in studying hydrate formation. In contrast, Molecular Dynamics (MD) simulations have been proven to be a useful tool for exploring these nanoscale processes (Bagherzadeh et al., 2013; Kondori et al., 2019; Zhang et al., 2022). Here, MD simulations were employed to study the secondary formation of methane with varied condition parameters, including residual structure size, temperature, and gas concentrations. The aims of this study are: (1) to investigate the interaction between methane molecules and hydrate residual structures; (2) to verify the microscopic mechanisms by which residual structures promote hydrate secondary formation by using methane hydrate; (3) to explore the synergy between residual structures and gas concentration during secondary formation. This study systematically analyzed the role of residual structures in hydrate secondary formation, which is essential for advancing the understanding of rapid hydrate reformation mechanisms and developing strategies to mitigate hydrate-induced pipeline blockage, thereby ensuring safe and efficient transportation.

2. Methodology

2.1. Model system and force-field parameters

Model systems consisting of gas, water, and residual structures with periodic boundary conditions were constructed to simulate the hydrate secondary formation, as an example shown in Fig. 1. The simulation box had a volume of $7.6 \times 7.6 \times 7.6$ nm^3. A typical system contained residual structures of different sizes, 6500 water molecules, and varied numbers of gas molecules. In this study, residual structures are defined as metastable hydrate-like clusters smaller than the critical size required for hydrate growth (Vysniauskas and Bishnoi, 1983). To obtain residual structures of different sizes, hydrate decomposition simulations were performed in advance using a pure methane hydrate system consisting of 2346 water molecules and 408 methane molecules. In this study, residual structures are defined as metastable hydrate-like structures smaller than the hydrate critical size, with the size represented by the number of comprising water molecules (Li et al., 2020). The critical size under 260 K and 300 bar is approximately 262 water molecules (as shown in Fig. S1). As a result, the residual structures of sizes ranging from 75 to 228 water

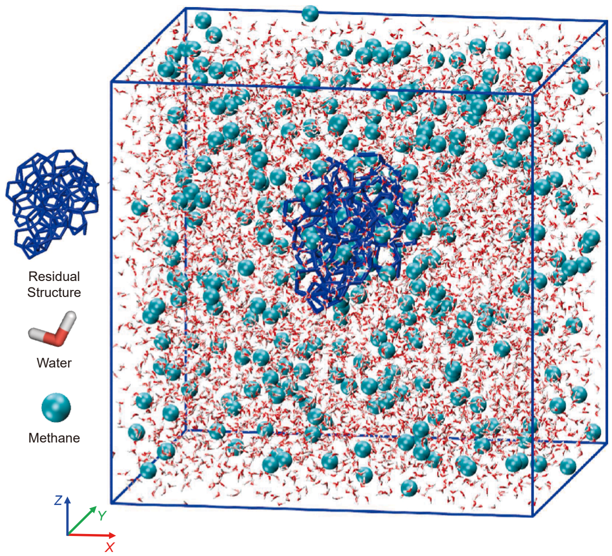

Fig. 1. The initial structure of an example methane-water well-mixed system. The system contains 6500 water molecules (red and white sticks for oxygen and hydrogen, respectively), 270 methane molecules (cyan spheres), and the residual structures (blue framework). The same color scheme was used in all figures if not otherwise specified.

molecules were used, and a hydrate structure containing 306 water molecules was used as the control group. The number of gas molecules contained in the residual structure is provided in Table S1. F4 order parameters of these clusters are shown in Fig. S2. The number of methane molecules used in this study ranged from 100 to 650 for the mole ratio of methane to water from 0.018 to 0.1. It is worth noting that the methane/water mole ratio of 0.035 was the maximum concentration at which no nanobubbles were observed in the system (shown in Fig. S3), and this ratio was considered as the saturation solubility of methane in the solution. All hydrate formation observed in the systems were secondary hydrate formation, as the water and gas had already been mixed and did not involve the lengthy mass transfer processes of primary hydrate formation. (Liang et al., 2022; Wen et al., 2021). Given that the pure methane hydrate systems used in this study mainly contain 5^{12} and $5^{12}6^2$ cages, the competition between different cage types is negligible. The number of water molecules identified as the hydrate structures was applied as the key parameter to characterize the hydrate formation process. This parameter directly indicates the size evolution of the hydrate structure and has been widely used to quantify hydrate nucleation and growth behaviors in previous research (Li et al., 2020; Zhang et al., 2025). The TIP4P-ICE model (Abascal et al., 2005) was used to describe the water molecules, and the OPLS-UA was employed to describe methane molecules (Jorgensen et al., 1984), respectively. Both models have been proven reliable in previous research (Blazquez et al., 2022; Linse and Hub, 2021; Martin, 2006).

2.2. Simulations

All the MD simulations were performed using Gromacs 2023.5 (Van Der Spoel et al., 2005). The initial system with periodic boundary conditions was first energy minimized using the steepest descent method and further relaxed by a short equilibration of 2 ns under the NVT ensemble at a temperature of 300 K. Position restraints were only applied to the residual structures during system preparation, namely during the energy minimized and pre-equilibration under the NVT ensemble to maintain their stability. The Newtonian equations of motion were integrated with the Velocity-Verlet algorithm (Molinero and Moore, 2009) with a time step of 2 fs. A cut-off distance of 1 nm was used to truncate the non-bonded interactions, with the long-range electrostatics treated by the Particle Mesh Ewald method (York et al., 1993) in all the simulations. The system was then subjected to simulations under the NPT ensemble, with the hydrate formation conditions of temperature in the range of 255–265 K and constant pressure of 300 bar (for methane). The Nosé-Hoover thermostat (Hoover, 1986) with a relaxation time of 0.4 ps was used to control the temperature and the Parrinello-Rahman (Parrinello and Rahman, 1980) algorithm with a relaxation time of 4 ps was employed to control the pressure. The individual simulation time ranged from 0.4 to 1.2 μs, depending on the complete formation of hydrates in the systems. Between 5 and 20 independent simulations were carried out to ensure each system for the statistical reproducibility and reliability of the results.

2.3. Umbrella sampling method

Umbrella sampling (Kästner, 2011) along the migration path of a methane molecule from the methane phase to the hydrate phase was conducted to analyze the free energy profile of methane diffusion. An extra system comprising approximately 5704 water atoms and 992 methane molecules for hydrate, 12000 atoms for water and 3000 atoms for methane phase was set up. The system is composed of gas, water, and hydrate structures with periodic boundary conditions, as shown in Fig. S4. An umbrella potential was applied to a selected methane molecule to probe its migration path through the methane phase towards the hydrate phase. The methane molecule positions along the *Z*-axis of the simulation box from 10 to 5 nm were chosen for umbrella sampling (as indicated in Fig. S4), with intervals of 0.2 nm. The umbrella potential used had a force constant of 500 $kJ \cdot mol^{-1} \cdot nm^{-2}$, following previous studies (Beckmann et al., 2015; Xiao et al., 2009). The sampling time was 30 ns for all the intervals. The potential of mean force was calculated using the weighted histogram analysis method (Kumar et al., 1992).

3. Result and discussion

3.1. “Adsorption-capture” of methane on hydrate structures

Methane molecules tend to adsorb onto and then be captured by hydrate structures, confirming its important role in the previously identified “memory effect” of quick hydrate reformation (Gao et al., 2023; Kou et al., 2022; Wen et al., 2021). As illustrated by the potential of mean force (PMF) by umbrella sampling in Fig. 2(a), methane molecules experience two dramatic free energy fluctuations on the path of mass transfer from the gas phase, through the water phase, to the hydrate growth interface. First, methane molecules need to cross the water-methane interface, overcoming an obvious energy barrier posted by the surface tension of water. Not only is the height of the energy significant (roughly 8 kJ/mol observed in the umbrella sampling system in Fig. 2(a)), but also the wall of the energy barrier at the gas–water interface is also highly steep (red region of Fig. 2(a)). Such energy barrier on the migration path of methane results in the limiting step of the long waiting time of the primary formation of hydrate (Veluswamy et al., 2020). In the aqueous phase, methane molecules diffuse on a rough free energy plateau, encountering minor fluctuations owing to colliding with water molecules (PMF in Fig. 2(a)). Interestingly, methane molecules experience an absorbing force in the vicinity of the hydrate surface, as depicted by the drastic decreasing trend of free energy in Fig. 2(a) (green

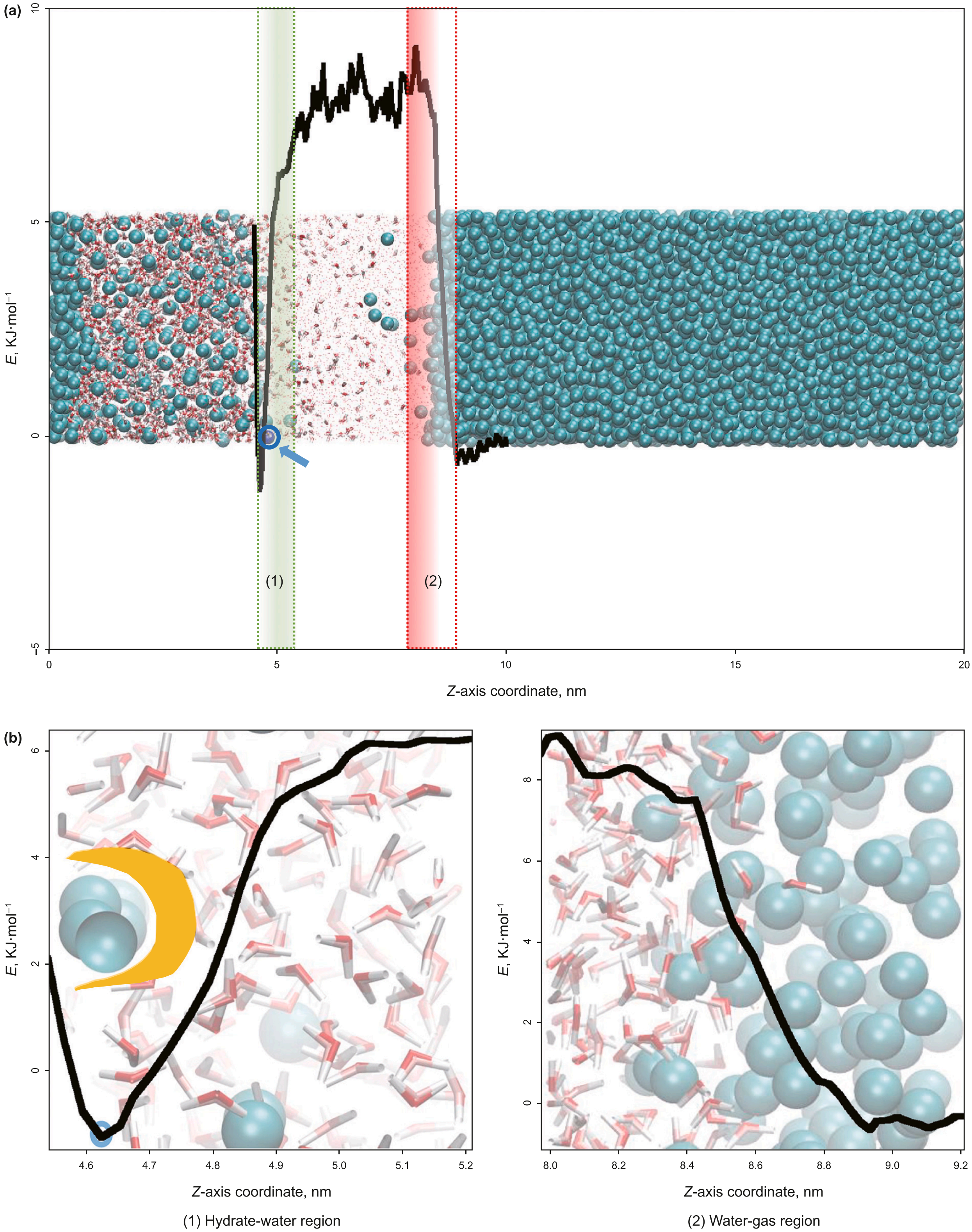

Fig. 2. Potential of Mean Force (PMF) on the migration path of methane molecules across the gas, water, and hydrate phases. **(a)** A typical PMF profile monitored during the migration of methane molecules from the methane phase through the aqueous phase to the hydrate crystal, with the corresponding system snapshots aligned with the observed energy barrier. The green and red shaded regions highlight the hydrate-water and water-gas interfaces, respectively. **(b)** Representative PMF profile and snapshots, corresponding to the circled numbers in (a), (1) represents the hydrate-water interface, with the "Venus flytrap" of water molecules capturing methane indicated by orange color. The blue circle indicates the bottom of the free energy well of the PMF profile (left panel), (2) represents the water-gas interface.

region). The region of decreasing free energy for methane molecules coincides with the quasi-liquid layer (QLL) on the hydrate surface, as confirmed by the instant displacement of water molecules shown in Fig. S5 (Zhang et al., 2024c). Methane molecules reaching the solid hydrate are captured at the hydrate surface as denoted by a deep free energy well (the green region of the PMF by umbrella sampling, Fig. 2(a)). To understand the energy well experienced by methane molecules, the microscopic structure of the hydrate-water interface was further analyzed.

As shown in Fig. 2(b)(1), as methane molecules approach the hydrate-water interface (blue circle in Fig. 2(b)(1)), they are stably captured within the cavity of a hydrate semi-cage featuring a "Venus flytrap" shape. The captured methane molecules do not migrate further into the solid hydrate, as a steep rising free energy barrier exists, as shown in Fig. 2(a), which is consistent with the accepted mass transfer limit of guest molecules into solid hydrates (Liang et al., 2022; You et al., 2019). To ensure that these findings were not limited to the structure shown in Fig. 2(a), free energy profiles across various hydrate sizes and positions were analyzed. The results, as depicted in Fig. S6, show consistent free energy profiles in each independent simulation. Given that hydrate residual structures are hydrates that are not fully melted and often contain key semi-cage or cup-like structures with strong affinity for methane molecules (Cheng et al., 2024; Oshima et al., 2010), the similar adsorption-capture behavior is expected at the residual structure interface.

3.2. *Effect of residual structure size on hydrate secondary formation*

The size of residual structures notably impacts the three stages of hydrate induction, nucleation, and growth during secondary formation (Zheng et al., 2022), leading to four different hydrate formation patterns as shown in Fig. 3(a). Firstly, without residual structures in the system, no hydrate formation was observed during the extended simulation time (Brown profile in exemplified 800 ns simulation time, Fig. 3(a)), mainly due to the low gas concentration and the absence of nucleation sites. With relatively small residual structures (75 water molecules, pink profiles shown in Fig. 3(a)), a long induction time was required for hydrate nucleation to occur (>520 ns). Small residual structures are expected to decompose within an extremely short duration (<1 ns observed in the simulations). The decomposition of small residual structures in return releases methane into the solution, which increases the gas concentration in the aqueous phase and raises the likelihood of collisions between methane and water molecules. For example, in the system with a residual structure containing 101 water molecules, the methane/water mole ratio increases to 0.0451 after the residual structure decomposes, which is higher than that of the system without residual structure (0.0423). The corresponding induction time decreased from over 800–250 ns, representing a reduction of up to 68.75%. Overall, the instability of small residual structures hinders the rapid secondary formation for hydrates.

In comparison, larger residual structures result in shorter induction times, as evidenced by the significantly reduced induction time (250 ns) for a residual structure with a size of 101 water molecules in Fig. 3(a) (blue profile). With even larger sizes (>157 water molecules), the residual structures do not decompose during the hydrate formation process but trigger hydrate formation already at the beginning of the simulations, as in Fig. 3(a). These large residual structures serve as nucleation sites, allowing hydrate to grow directly on their surfaces. The large residual structures are also sufficiently stable for the 'adsorption-capture' of methane molecules, as discussed above. In the vicinity of the large residual structures, a local supersaturation region of methane was observed during the simulation, which agrees with the results previously reported (Zhang et al., 2025). The large residual structures result in a short nucleation stage, and the larger the residual structure size, the shorter the nucleation duration (green and red profiles in Fig. 3(a)). With the residual structure size exceeds the critical size (black profile in Fig. 3(a)), hydrate growth in the system skips the nucleation stage and directly enters the growth stage. The results thus confirm that residual structures promote secondary formation via two key approaches: (1) by adsorbing and capturing methane molecules, acting as the nucleation sites, and (2) by releasing methane molecules through decomposition, thereby increasing the gas concentration in the system.

Because the stability of residual structures is determined by temperature, one of the most critical factors known for impacting hydrate growth (Yin et al., 2018), the secondary hydrate formation patterns observed above are also affected by temperature. Despite

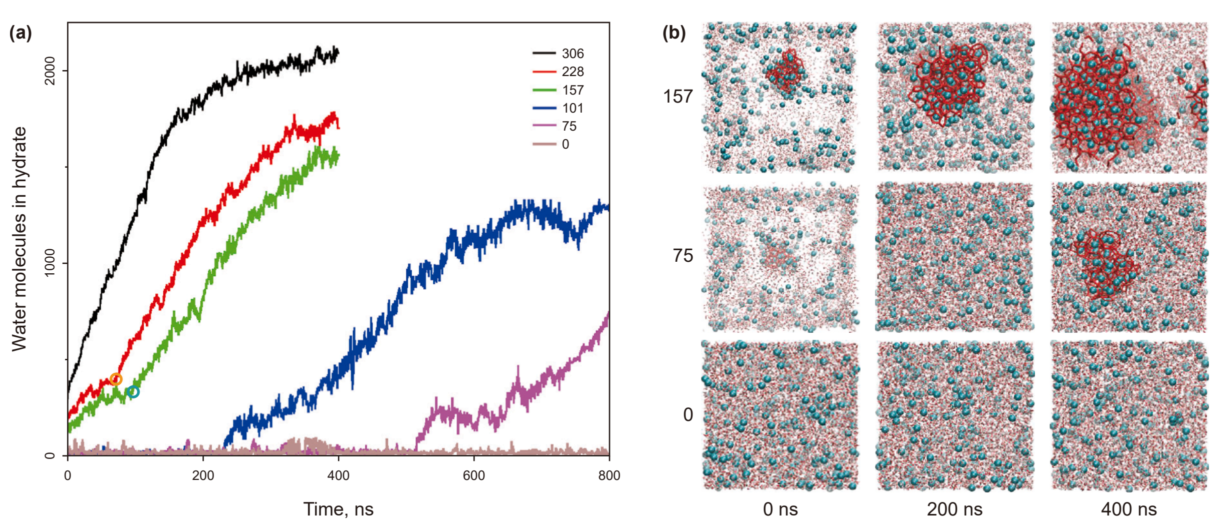

Fig. 3. Effect of residual structure size on the hydrate secondary formation. **(a)** Hydrate size profiles during secondary formation under different residual structure sizes with 0.042 methane/water mole ratio under 265 K and 300 bar. The number of water molecules in the residue structure is taken as the size of the residual structure (Li et al., 2020). The residual structure sizes in the initial systems are given as legends. Each profile is the average of 5–10 independent simulations. **(b)** Representative system snapshots during secondary formation with different sizes of residual structure of 0, 101 and 157 water molecules. The hydrate structures are indicated by blue rods.

that the four formation patterns observed at 265 K (Fig. 3(a)) also appear at different temperature as shown in Fig. S7, the same residual structure, yet can lead to varied hydrate growth patterns under different temperature. For example, the residual structure with a size of 157 water molecules enables hydrate formation directly at 255K first decomposes and releases methane, then triggers hydrate formation by increasing methane concentration at 265 K (Fig. S8). The result suggests that the absolute size of the residual structure is not the only decisive factor of the hydrate secondary formation. It is worth noting that the residual structures here are chosen to have sizes smaller than the critical size of hydrate structures that can trigger hydrate growth (Liu et al., 2021a; Zhang et al., 2025), the critical size however varies significantly with temperature as shown by Fig. 4(a) and Fig. S1. The definition of hydrate critical size refers to the hydrate size that enables the system to enter the growth stage. As such, the R/C value is defined as the ratio of the residual structure size to the critical size required for hydrate nucleation. It is used to identify how residual structures may promote secondary hydrate formation, given that their stability is strongly size-dependent, as shown in Fig. 4(b). Notably, residual structures with R/C ratio greater than 60% are found to serve as a nucleation site, while those with R/C below 25% decompose in the simulations. With an increasing R/C ratio in the range of 25%–60%, residual structures demonstrate gradually raised probability from decomposing to serve as nucleation sites. Interestingly, the probability of residual structures serving as nucleation sites rapidly increases as the R/C ratio is close 40%, (green box, Fig. 5(b)). The results thus indicate that residual structures with sizes reach 40% of the critical size can strongly promote the secondary formation act as nucleation sites. Otherwise, residual structures smaller than 40% of the critical size tend to decompose, enhancing hydrate secondary formation by increasing the gas concentration in the system.

3.3. *Effect of gas concentration on residual structure stability and formation behavior*

Being another crucial factor in hydrate formation, gas concentration in the system significantly influences the nucleation around residual structures. High methane concentration increases the likelihood of residual structures acting as nucleation sites, as results shown in Fig. 5(a). Methane concentration determines the metastable state of residual structures towards either decomposing or serving as nucleation sizes. For example, low methane concentration leads to residual structure decomposition (Fig. 5(b)(2)), while high methane concentration results in nucleation and hydrate growth of the same residual structure (Fig. 5(b)(1)). With the higher methane concentration, the more methane molecules are absorbed on the residual structures as shown in Fig. S9. Importantly, a high methane concentration in the system results in the local gas-supersaturated formation in the vicinity of the residual structure, which was found highly favored for hydrate growth as reported in previous studies (Zhang et al., 2025). Moreover, higher gas concentration results in a smaller residual structure size required to act as nucleation sites, as shown in Table S2. For example, in systems with methane concentration of methane/water mole ratio of 0.018, residual structure of 306 water molecules is needed to trigger hydrate nucleation. In comparison, with methane concentration of methane/water mole ratio reaches 0.058, residual structures with only 75 water molecules can already promote hydrate nucleation and growth. For stable large residual structures exceeding the critical size, a relatively low methane concentration is needed for hydrate growth, thanks to the “adsorption-capture” effect discussed above. For example, in systems with residual structures of 306 water molecules, the methane concentration required for hydrate growth is 0.023 methane/water mole ratio, which is lower than the methane

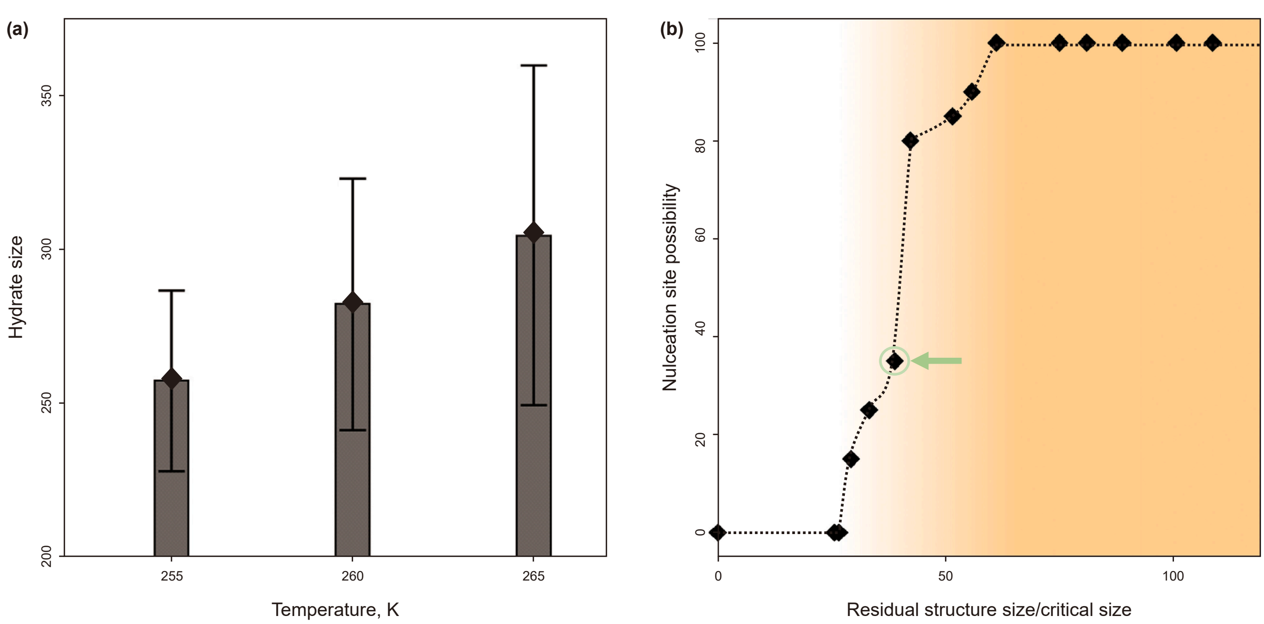

Fig. 4. Effect of critical size in determining hydrate formation pattern. **(a)** Hydrate critical size at different temperatures. The result shown here was obtained from the system with the methane/water mole ratio of 0.042. The error bars are the standard deviation of 5 independent simulations. **(b)** The probability of residual structures as nucleation sites at different R/C ratios. The probability was calculated by normalizing the number of occurrences of residual structures as nucleation sites by the total number of simulations and was obtained from the 10–20 independent simulations of all the systems with varied R/C ratios under different temperature. The R/C ratio leading to obvious raised probability of residual structures as nucleation sites is indicated by the green circle and arrow. The same calculation method is used in the results of the following figures if not otherwise specified.

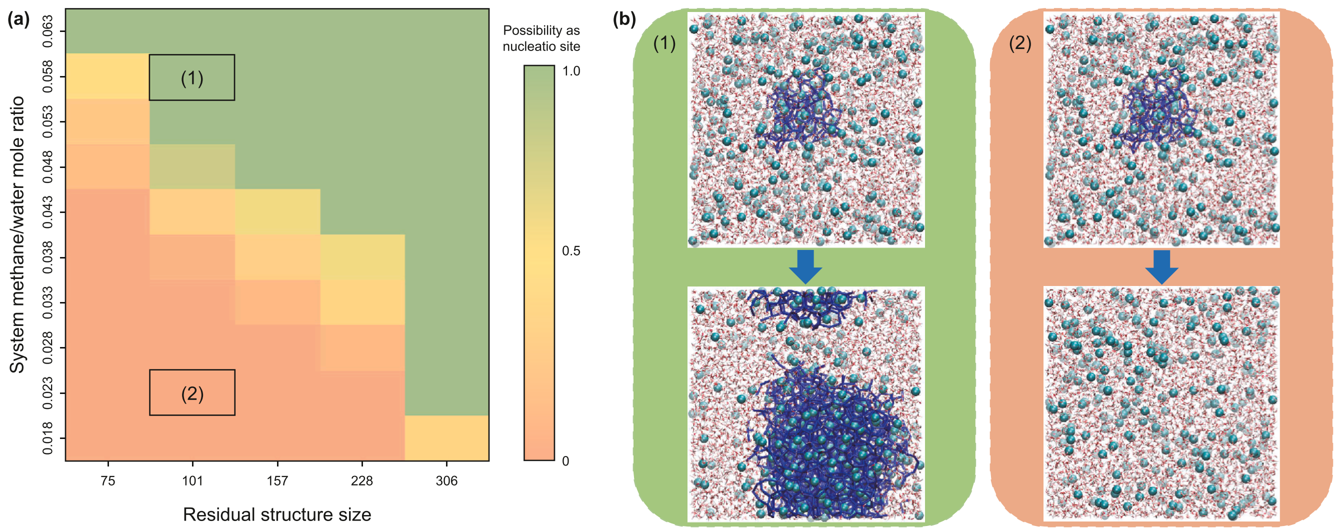

Fig. 5. The effect of gas concentration on stability and nucleation behavior of residual structure. (**a**) The probability of the residual structure of varied sizes acting as nucleation sites in systems with different methane concentrations under 260 K and 300 bar. The probability is represented by different colors, with color schemes shown in the scale bar. The nucleation probability of each residual structure was obtained from the 10–20 independent simulations. (**b**) Representative snapshots of residual structures triggering hydrate nucleation (left panel) and decomposing (right panel) observed in the simulations, with circled numbers highlighted in (a). The simulation time in both cases is 400 ns, as indicated by the arrows.

saturation solubility (0.035 as mentioned in section 2.1). Indeed, low methane concentration in the system does not hinder the “adsorption-capture” effect on methane molecules by the large and stable residual structures nor the resulting high local concentration (Fig. 6) important for hydrate growth. It is worth noting that previous molecular dynamics simulation studies have found gas saturation to be crucial for hydrate growth (Ma et al., 2020). The results here further suggest that methane-unsaturated solutions can also exhibit hydrate secondary formation as long as the residual structures are sufficiently large, which extends the current understanding of hydrate formation.

Interestingly, a stably high local methane concentration is observed in the vicinity of residual structures of all sizes, as shown in Fig. 6. Specifically, the local methane concentration within the nucleation region remains stable at roughly 0.081 methane/water mole ratio (black dashed lines and dots, Fig. 6(a)), regardless of the residual structure size. The initial growth region is defined by the first solvation shell of the

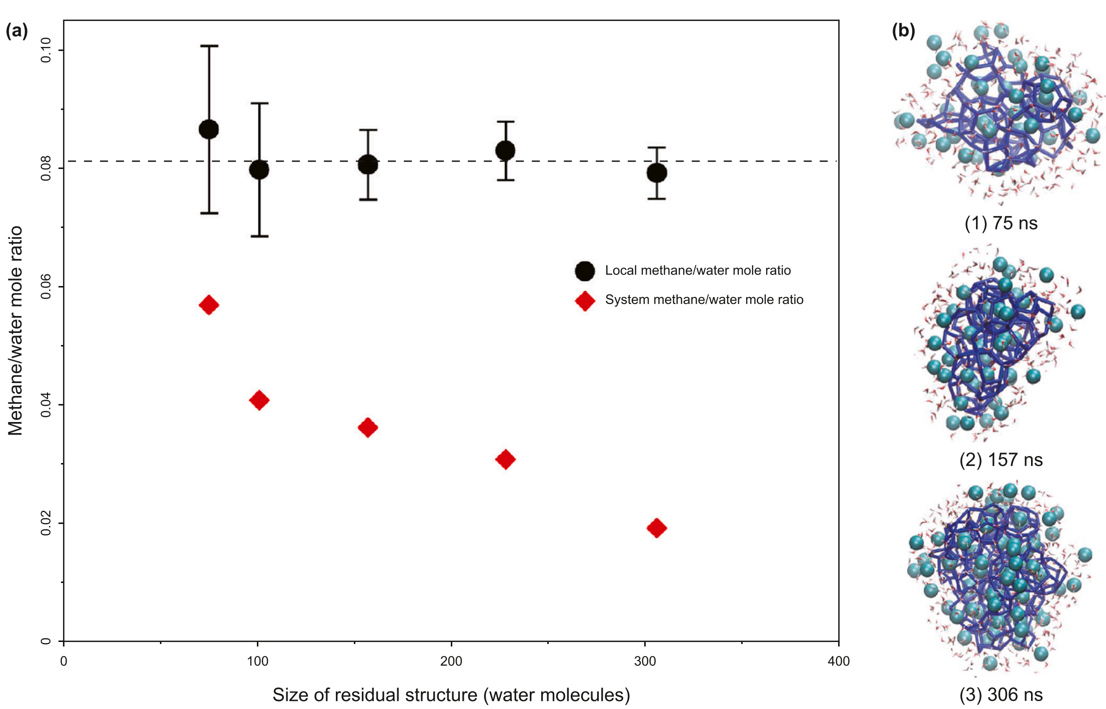

Fig. 6. Stable local gas concentration on residual structures. (**a**) Local methane/water mole ratio in the vicinity of residual structures of different sizes during hydrate formation shown in black, with the average shown by the black dashed line. The corresponding system methane concentration is shown in red. The error bars are the standard deviation of 5 independent simulations. (**b**) Typical snapshots of residual structures of varied sizes with local methane molecules on their surfaces observed in the simulations.

hydrate structure, the range of which is determined by the radial distribution function (RDF) between methane and water molecules, with the first peak located at approximately 0.473 nm (shown in Fig. S10). The stably high local methane concentration monitored is largely attributed to the 'adsorption-capture' effect in the hydrate nucleation and growth process, despite the overall system methane concentration decreases with increasing residual structure sizes (red diamonds, Fig. 6(a)). Again, the sufficiently high local methane concentration is enabled by stable residual structures providing sites for gas adsorption and capture on their surfaces Fig. 6(b)), even in systems with the overall gas concentration significantly below saturation. It is worth noting that this local methane concentration is influenced by key parameters such as temperature and pressure and may present differences in different systems.

3.4. Shortened induction time by the synergy of residual structures and gas supersaturation

The induction time of hydrate formation is shortened with the presence of residual structures and an optimal gas concentration, as well as the synergy between these two. As shown in Fig. 7(a), the induction time monitored follows a U-shaped trend in systems without residual structures with increasing methane concentrations (red profile, Fig. 7(a)), in consistence with previous studies (Zhang et al., 2025). With residual structures in the systems, the induction time exhibits an L-shaped trend, characterized by a rapid decrease followed by stable low values at high gas concentrations (black profile, Fig. 7(a)). Specifically, long induction time with large standard deviation was observed in systems with methane/water mole ratio lower than 0.044. The high fluctuation in the induction time monitored in these systems can be attributed to the high probability of residual structures decomposing and reforming at lower methane concentrations. With the methane/water mole ratio exceeding 0.044, the induction time maintains at a low plateau with high significance (small standard deviation, black profile, Fig. 7(a)), which sharply contrasts with extended induction time due to nanobubble formation in systems without residual structures (Fig. S11 and red profile, Fig. 7(a)). The induction time is not further reduced with higher gas concentration, largely because the surface area of the residual structure reaches its capacity to adsorb methane molecules, despite of increasing gas concentration.

The difference in the induction time (Δt) between systems with and without residual structure presents a reference for the understanding of the synergy effect of the optimal gas concentration and residual structures. As illustrated in Fig. 7(b), Δt also exhibits a U-shaped trend as methane concentration increases, with a minimum at the 0.062 methane/water mole ratio. At lower methane concentrations, Δt is considerably large due to the significant effect of residual structures in promoting hydrate formation. However, induction time can be reduced both by increased system gas concentration and the presence of residual structure as results shown in Fig. 7(a). With system gas concentration in the range of 0.042–0.062, Δt approaches its minimum (green arrow, Fig. 7(b)) owing to the most obvious effect of gas concentration in reducing induction time. As the gas concentration continues to rise, Δt increases, highlighting the synergy of gas concentration and residual structures. In systems without residual structure, induction time is extended due to the formation of nanobubbles in systems (Fig. S11). In contrast, short induction time is maintained in systems with residual structures, thanks to the synergy effect with residual structure for the 'adsorption-capture' of methane molecules and high gas concentration providing ample methane molecules for hydrate nucleation and growth. This observation is consistent with the viewpoint proposed in previous studies (He et al., 2024). The results here indicate that residual structures and gas supersaturation can jointly promote the formation of local gas-supersaturation regions, thereby facilitating hydrate formation.

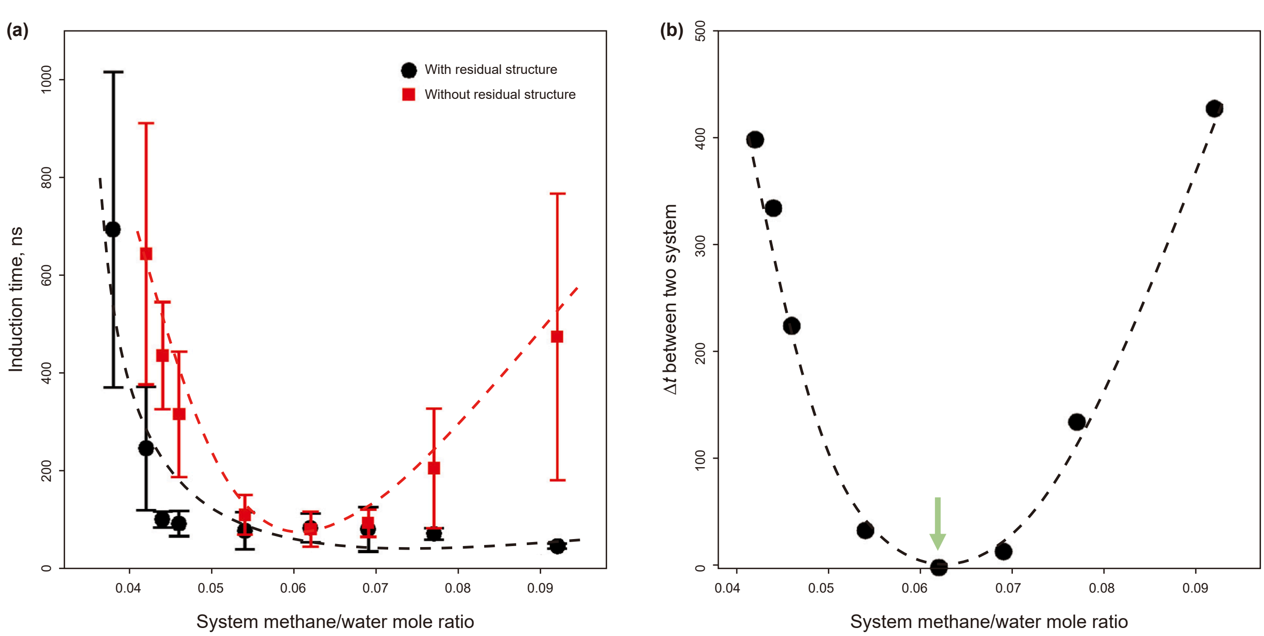

Fig. 7. The synergy of gas concentration and residual structures on the secondary formation of hydrates. **(a)** Hydrate formation induction time in systems with varied methane/water mole ratios with (black) and without (red) residual structures. The results shown here are obtained with residual structure with sizes of 157 water molecules. The error bars show the standard deviation of the results from 5 independent simulations. **(b)** The difference in induction time between systems of the same gas concentration with and without residual structures shown in (a). The minimum is indicated by the green arrow.

4. Conclusions

This study employed molecular dynamics simulations to systematically investigate the microscopic promotion mechanism of residual structures on hydrate secondary formation at the nanoscale. The effects of system temperature and gas concentrations were also analyzed to explore their potential in flow assurance strategies. The results show that, due to their 'Venus flytrap' shape, residual structures exhibit an "adsorption-capture" effect on free gas molecules. This effect significantly increases the local methane concentration around the residual structures, thereby promoting the formation of hydrates.

Furthermore, the study revealed that the ratio of residual structure size to critical size may determine the hydrate formation patterns. Under the present simulation conditions, this threshold is about 40%, but this value will be affected by environmental factors such as pressure, temperature, and initial methane concentration. When the R/C value exceeds threshold, the residual structure can remain stable and act as a nucleation site, while smaller ones decompose and release gas, thereby increasing the overall gas concentration. Moreover, a significant synergistic effect was observed between residual structures and gas concentrations: high gas concentrations enhance the stability of small residual structures, enabling them to serve as nucleation sites, while stable large residual structures can enrich gas molecules even under low overall gas concentrations, forming local gas supersaturated regions that promote hydrate secondary formation.

This work offers new microscopic insights into the hydrate memory effect by revealing the dual role of residual structures in promoting secondary formation, thereby addressing current limitations in experimental investigations. These findings provide theoretical support for flow assurance strategies in oil and gas transportation systems and call for future collaborative experimental validation, to pave the way to the safe and sustainable development of offshore oil and gas resources.

CRediT authorship contribution statement

Yi-Fan Zhang: Writing – review & editing, Writing – original draft, Visualization, Validation, Software, Methodology, Investigation, Formal analysis, Data curation, Conceptualization. **Sen-Bo Xiao:** Writing – review & editing, Visualization, Validation, Supervision, Software, Methodology, Investigation, Conceptualization. **Zhi-Liang Zhang:** Writing – review & editing, Supervision, Funding acquisition, Conceptualization. **Jian-Ying He:** Writing – review & editing, Supervision, Resources, Project administration, Investigation, Conceptualization.

Declaration of competing interest

The authors declare that they have no known competing financial interests or personal relationships that could have appeared to influence the work reported in this paper.

Acknowledgments

We are grateful for the support of the Research Council of Norway through the D'andra project (Grant No. 302348). The supercomputer CPU hours were provided by the Norwegian Metacenter for Computational Science (Grant No. NN9110K, NN9391K, and NN8084K).

Appendix A. Supplementary data

Supplementary data to this article can be found online at https://doi.org/10.1016/j.petsci.2025.11.017.

References

Abascal, J., Sanz, E., García Fernández, R., Vega, C., 2005. A potential model for the study of ices and amorphous water: TIP4P/Ice. J. Chem. Phys. 122, 234511. https://doi.org/10.1063/1.1931662.

Bagherzadeh, S.A., Alavi, S., Ripmeester, J.A., Englezos, P., 2013. Evolution of methane during gas hydrate dissociation. Fluid Phase Equilib. 358, 114–120. https://doi.org/10.1016/j.fluid.2013.08.017.

Beckmann, A., Xiao, S.B., Müller, J.P., Mercadante, D., Nüchter, T., Kröger, N., Langhojer, F., Petrich, W., Holstein, T.W., Benoit, M., Gräter, F., Özbek, S., 2015. A fast recoiling silk-like elastomer facilitates nanosecond nematocyst discharge. BMC Biol. 13, 1–16. https://doi.org/10.1186/s12915-014-0113-1.

Blazquez, S., Conde, M., Abascal, J., Vega, C., 2022. The Madrid-2019 force field for electrolytes in water using TIP4P/2005 and scaled charges: extension to the ions F^-, Br^-, I^-, Rb^+, and Cs^+. J. Chem. Phys. 156, 044505. https://doi.org/10.1063/5.0077716.

Buchanan, P., Soper, A.K., Thompson, H., Westacott, R.E., Creek, J.L., Hobson, G., Koh, C.A., 2005. Search for memory effects in methane hydrate: structure of water before hydrate formation and after hydrate decomposition. J. Chem. Phys. 123, 164507. https://doi.org/10.1063/1.2074927.

Chen, Y.C., Gong, J., Shi, B.H., Yao, H.Y., Liu, Y., Fu, S.K., Song, S.F., Lv, X.F., Wu, H.H., Lou, X., 2020. Investigation into methane hydrate reformation in water-dominated bubbly flow. Fuel 263, 116691. https://doi.org/10.1016/j.fuel.2019.116691.

Cheng, L., He, R.Z., Cui, J.L., Yi, Q., Liu, B., Chen, G.J., 2026. Microscopic insights into the fading mechanism of the hydrate memory effect. Fuel 404, 136212. https://doi.org/10.1016/j.fuel.2025.136212.

Cheng, L., Li, Y.F., Cui, J.L., Qin, H.B., Ning, F.L., Liu, B., Chen, G.J., 2024. Molecular simulation study on the evolution process of hydrate residual structures into hydrate. Chin. J. Chem. Eng. 69, 79–91. https://doi.org/10.1016/j.cjche.2023.12.023.

Cook, M., 2021. Trends in global energy supply and demand. Dev. Pet. Sci. 15–42. https://doi.org/10.1016/B978-0-12-821190-8.00002-2.

Dyatlov, S., Didenko, N., Ivanova, E., Soshneva, E., Kulik, S., 2020. Prospects for alternative energy sources in global energy sector. IOP Conf. Ser.: Earth Environ. Sci. 434, 012014. https://doi.org/10.1088/1755-1315/434/1/012014.

Gao, Q., Zhao, J.Z., Guan, J., Zhang, C., 2023. Influence of the memory effect during CO2/CH4 mixed gas hydrate reformation process. Fuel 353, 129249. https://doi.org/10.1016/j.fuel.2023.129249.

Gao, Y., Dai, L.K., Zhu, H.D., et al., 2019. Quantitative analysis of main components of natural gas based on Raman spectroscopy. Chin. J. Anal. Chem. 47 (1), 67–76. https://doi.org/10.1016/S1872-2040(18)61135-1.

Haider, W.H., 2020. Estimates of total oil & gas reserves in the world, future of oil and gas companies and smart investments by E & P companies in renewable energy sources for future energy needs. https://doi.org/10.2523/IPTC-19729-MS.

Hassanpouryouzband, A., Joonaki, E., Farahani, M.V., Takeya, S., Ruppel, C., Yang, J.H., English, N.J., Schicks, J.M., Edlmann, K., Mehrabian, H., Aman, Z.M., Tohidi, B., 2020. Gas hydrates in sustainable chemistry. Chem. Soc. Rev. 49 (15), 5225–5309. https://doi.org/10.1039/C8CS00989Aa.

He, Z.J., Jiang, J.W., Jiang, G.S., Ning, F.L., 2024. Competition between CH_4 hydrate formation and phase separation in a wetted metal–organic framework MIL-101 at moderate subcooling: molecular insights into CH_4 storage. J. Mater. Chem. A. 12 (8), 4447–4459. https://doi.org/10.1039/D3TA06952D.

Hoover, W.G., 1986. Constant-pressure equations of motion. Phys. Rev. A. 34 (3), 2499. https://doi.org/10.1103/PhysRevA.34.2499.

Jorgensen, W.L., Madura, J.D., Swenson, C.J., 1984. Optimized intermolecular potential functions for liquid hydrocarbons. J. Am. Chem. Soc. 106 (22), 6638–6646. https://doi.org/10.1021/ja00334a030.

Karaaslan, U., Uluneye, E., Parlaktuna, M., 2002. Effect of an anionic surfactant on different type of hydrate structures. J. Pet. Sci. Eng. 35 (1–2), 49–57. https://doi.org/10.1016/S0920-4105(02)00163-8.

Kästner, J., 2011. Umbrella sampling. Wiley Interdiscip. Rev. Comput. Mol. Sci. 1 (6), 932–942. https://doi.org/10.1002/wcms.66.

Kim, H., Kim, J., Seo, Y., 2020. Economic benefit of methane hydrate reformation management in transport pipeline by reducing thermodynamic hydrate inhibitor injection. J. Pet. Sci. Eng. 184, 106498. https://doi.org/10.1016/j.petrol.2019.106498.

Kondori, J., Zendehboudi, S., James, L., 2019. New insights into methane hydrate dissociation: utilization of molecular dynamics strategy. Fuel 249, 264–276. https://doi.org/10.1016/j.fuel.2019.02.125.

Kou, X., Feng, J.C., Li, X.S., Wang, Y., Chen, Z.Y., 2022. Memory effect of gas hydrate: influencing factors of hydrate reformation and dissociation behaviors. Appl. Energy 306, 118015. https://doi.org/10.1016/j.apenergy.2021.118015.

Kumar, S., Rosenberg, J.M., Bouzida, D., Swendsen, R.H., Kollman, P.A., 1992. The weighted histogram analysis method for free-energy calculations on biomolecules. I. The method. J. Comput. Chem. 13 (8), 1011–1021. https://doi.org/10.1002/jcc.540130812.

Kvamme, B., Aromada, S.A., Saeidi, N., Hustache-Marmou, T., Gjerstad, P., 2020. Hydrate nucleation, growth, and induction. ACS Omega 5 (6), 2603–2619. https://doi.org/10.1021/acsomega.9b02865.

Li, L.W., Zhong, J., Yan, Y.G., Zeng, X.C., 2020. Unraveling nucleation pathway in methane clathrate formation. Proc. Natl. Acad. Sci. U. S. A 117 (40), 24701–24708. https://doi.org/10.1073/pnas.2011755117.

Li, Y.L., Ning, F.L., Xu, M., Qi, H.M., Sun, J.X., Nouri, A., Gao, D.L., Wu, N.Y., 2023. Experimental study on solid particle migration and production behaviors during marine natural gas hydrate dissociation by depressurization. Pet. Sci. 20 (6), 3610–3623. https://doi.org/10.1016/j.petsci.2023.05.018.

Liang, H.Y., Guan, D.W., Shi, K.J., Yang, L., Zhang, L.X., Zhao, J.F., Song, Y.C., 2022. Characterizing mass-transfer mechanism during gas hydrate formation from water droplets. Chem. Eng. J. 428, 132626. https://doi.org/10.1016/j.cej.2021.132626.

Linse, J.-B., Hub, J.S., 2021. Three-and four-site models for heavy water: SPC/E-HW, TIP3P-HW, and TIP4P/2005-HW. J. Chem. Phys. 154, 194501. https://doi.org/10.1063/5.0050841.

Liu, Y., Lv, X.F., Ma, Q.L., Zhou, S.D., Shi, B.H., Du, H., Lei, Y., Yu, P.F., Song, S.F., Gong, J., Sun, B.C., 2022. Investigation on synergistic deposition of wax and hydrates in waxy water-in-oil (W/O) flow systems. Pet. Sci. 19 (4), 1840–1852. https://doi.org/10.1016/j.petsci.2022.04.004.

Liu, Z., Li, Y.X., Wang, W.C., Song, G.C., Lu, Z.Y., Ning, Y.X., Liu, S., 2021a. Experimental investigation on the micro-morphologies and growing process of methane hydrate formation in SDS solution. Fuel 293, 120320. https://doi.org/10.1016/j.fuel.2021.120320.

Liu, Z., Sun, B., Wang, Z., Zhang, J., Wang, X., 2021b. Prediction and management of hydrate reformation risk in pipelines during offshore gas hydrate development by depressurization. Fuel 291, 120116. https://doi.org/10.1016/j.fuel.2020.120116.

Lv, X., Li, C., Liu, Y., Peng, M.G., Wang, C.S., Ma, Q.L., Zhou, S.D., Li, X.Y., Shi, B.H., Song, S.F., 2024. Study on the hydrate growth characteristics and rheology of silica-containing sand water-in-oil emulsion system. Fuel 374, 132438. https://doi.org/10.1016/j.fuel.2024.132438.

Ma, R., Zhong, H., Li, L.W., Zhong, J., Yan, Y.G., Zhang, J., Liu, J.X., 2020. Molecular insights into the effect of a solid surface on the stability of a hydrate nucleus. J. Phys. Chem. C. 124 (4), 2664–2671. https://doi.org/10.1021/acs.jpcc.9b09704.

Maeda, N., Wells, D., Hartley, P.G., Kozielski, K.A., 2012. Statistical analysis of supercooling in fuel gas hydrate systems. Energy Fuels 26 (3), 1820–1827. https://doi.org/10.1021/ef201965z.

Martin, M.G., 2006. Comparison of the AMBER, CHARMM, COMPASS, GROMOS, OPLS, TraPPE and UFF force fields for prediction of vapor–liquid coexistence curves and liquid densities. Fluid Phase Equilib. 248 (1), 50–55. https://doi.org/10.1016/j.fluid.2006.07.014.

Mo, F., Qi, Z.L., Huang, X.L., Li, Q.P., Yan, W.D., Wang, S., 2022. Pressure prediction in deep-water pipeline considering formation of natural gas hydrate. Front. Earth Sci. 10, 987594. https://doi.org/10.3389/feart.2022.987594.

Molinero, V., Moore, E.B., 2009. Water modeled as an intermediate element between carbon and silicon. J. Phys. Chem. B. 113 (13), 4008–4016. https://doi.org/10.1021/jp805227c.

Moon, C., Taylor, P.C., Rodger, P.M., 2003. Molecular dynamics study of gas hydrate formation. J. Am. Chem. Soc. 125 (16), 4706–4707. https://doi.org/10.1021/ja028537v.

Oshima, M., Shimada, W., Hashimoto, S., Tani, A., Ohgaki, K., 2010. Memory effect on semi-clathrate hydrate formation: a case study of tetragonal tetra-n-butyl ammonium bromide hydrate. Chem. Eng. Sci. 65 (20), 5442–5446. https://doi.org/10.1016/j.ces.2010.07.019.

Parrinello, M., Rahman, A., 1980. Crystal structure and pair potentials: a molecular-dynamics study. Phys. Rev. Lett. 45 (14), 1196. https://doi.org/10.1103/PhysRevLett.45.1196.

Roozeboom, H.W.B., 1884. Sur l'hydrate de chlore. Recl. Trav. Chim. Pays-Bas 3 (2), 59–72. https://doi.org/10.1002/recl.18840030203.

Sadeh, E., Farhadian, A., Stoporev, A.S., Semenov, M.E., Chirkova, Y.F., Naeiji, P., Varfolomeev, M.A., 2024. Methane Storage as a Hydrate, Advances and Technology Development in Greenhouse Gases: Emission, Capture and Conversion, pp. 275–321. https://doi.org/10.1016/B978-0-443-19067-4.00001-2.

Sayani, J.K.S., Pedapati, S.R., Lal, B., 2020. Phase behavior study on gas hydrates formation in gas dominant multiphase pipelines with crude oil and high CO_2 mixed gas. Sci. Rep. 10 (1), 14748. https://doi.org/10.1038/s41598-020-71509-6.

Seo, Y., Kang, S.P., 2012. Inhibition of methane hydrate re-formation in offshore pipelines with a kinetic hydrate inhibitor. J. Pet. Sci. Eng. 88, 61–66. https://doi.org/10.1016/j.petrol.2011.11.001.

Shi, B.H., Song, S.F., Chen, Y.C., Duan, X., Liao, Q.Y., Fu, S.K., Liu, L.H., Sui, J.H., Jia, J.P., Liu, H.T., Zhu, Y.M., Song, C.X., Lin, D.C., Wang, T., Wang, J.A., Yao, H.Y., Gong, J., 2021. Status of natural gas hydrate flow assurance research in China: A review. Energy Fuels 35 (5), 3611–3658. https://doi.org/10.1021/acs.energyfuels.0c04209.

Sloan Jr, E.D., Koh, C.A., 2007. Clathrate Hydrates of Natural Gases. CRC press.

Van Der Spoel, D., Lindahl, E., Hess, B., Groenhof, G., Mark, A.E., Berendsen, H.J.C., 2005. GROMACS: fast, flexible, and free. J. Comput. Chem. 26 (16), 1701–1718. https://doi.org/10.1002/jcc.20291.

Veluswamy, H.P., Bhattacharjee, G., Liao, J., Linga, P., 2020. Macroscopic kinetic investigations on mixed natural gas hydrate formation for gas storage application. Energy Fuels 34 (12), 15257–15269. https://doi.org/10.1021/acs.energyfuels.0c01862.

Vysniauskas, A., Bishnoi, P., 1983. A kinetic study of methane hydrate formation. Chem. Eng. Sci. 38 (7), 1061–1072. https://doi.org/10.1016/0009-2509(83)80027-X.

Wang, J.G., Meng, Y., Han, B.Y., Liu, Z.X., Zhang, L.X., Yao, H.Y., Wu, Z., Chu, J.W., Yang, L., Zhao, J.F., Song, Y.C., 2023a. Hydrate blockage in subsea oil/gas flowlines: prediction, prevention, and remediation. Chem. Eng. J. 461, 142020. https://doi.org/10.1016/j.cej.2023.142020.

Wang, X.H., Xu, X.J., Cai, J., Zheng, H.X., Li, X.X., Pang, W.X., Sun, C.Y., Chen, G.J., 2023b. Effect of residual guest concentration in aqueous solution on hydrate reformation kinetics. Fuel 339, 126923. https://doi.org/10.1016/j.fuel.2022.126923.

Wang, Y., Dong, S.Q., Zhang, M.D., Wu, Q.B., Zhang, X.M., Zhang, P., Zhan, J., 2020. Experimental study of the formation rate and distribution of methane hydrate in layered sand. ACS Omega 5 (46), 29882–29888. https://doi.org/10.1021/acsomega.0c03984.

Wei, Y., Maeda, N., 2023. Mechanisms of the memory effect of clathrate hydrates. Chem. Eng. Sci. 270, 118538. https://doi.org/10.1016/j.ces.2023.118538.

Wen, Z., Yao, Y., Luo, W., Lei, X., 2021. Memory effect of CO_2-hydrate formation in porous media. Fuel 299, 120922. https://doi.org/10.1016/j.fuel.2021.120922.

Wu, Q., Zhang, B., 2010. Memory effect on the pressure-temperature condition and induction time of gas hydrate nucleation. J. Nat. Gas Chem. 19 (4), 446–451. https://doi.org/10.1016/S1003-9953(09)60086-4.

Xiao, S., Stacklies, W., Cetinkaya, M., Markert, B., Gräter, F., 2009. Mechanical response of silk crystalline units from force-distribution analysis. Biophys. J. 96 (10), 3997–4005. https://doi.org/10.1016/j.bpj.2009.02.052.

Yin, Z., Khurana, M., Tan, H.K., Linga, P., 2018. A review of gas hydrate growth kinetic models. Chem. Eng. J. 342, 9–29. https://doi.org/10.1016/j.cej.2018.01.120.

York, D.M., Darden, T.A., Pedersen, L.G., 1993. The effect of long-range electrostatic interactions in simulations of macromolecular crystals: a comparison of the Ewald and truncated list methods. J. Chem. Phys. 99 (10), 8345–8348. https://doi.org/10.1063/1.465608.

You, K., Flemings, P.B., Malinverno, A., Collett, T., Darnell, K., 2019. Mechanisms of methane hydrate formation in geological systems. Rev. Geophys. 57 (4), 1146–1196. https://doi.org/10.1029/2018RG000638.

Zeng, H., Wilson, L.D., Walker, V.K., Ripmeester, J.A., 2006. Effect of antifreeze proteins on the nucleation, growth, and the memory effect during tetrahydrofuran clathrate hydrate formation. J. Am. Chem. Soc. 128 (9), 2844–2850. https://doi.org/10.1021/ja0548182.

Zhang, A.Y., Cai, M., Wei, N., Li, T.H., Zhang, C., Pei, J., Wang, X.W., 2024a. Analysis of sensitivity to hydrate blockage risk in natural gas gathering pipeline. Pet. Sci. 21 (4), 2723–2733. https://doi.org/10.1016/j.petsci.2024.01.016.

Zhang, J., Fu, H.Q., Guo, M.Z., Wang, Z., Li, L.W., Yin, Q., Yan, Y.G., Wei, W., Han, W.F., Zhong, J., 2024b. New insights into the deposition of natural gas hydrate on pipeline surfaces: a molecular dynamics simulation study. Pet. Sci. 21 (1), 694–704. https://doi.org/10.1016/j.petsci.2023.08.027.

Zhang, Y., Xiao, S., Ma, R., Zhang, Z., He, J., 2024c. Characterization of the quasi-liquid layer on gas hydrates with molecular dynamics simulations. Fuel 357, 129905. https://doi.org/10.1016/j.fuel.2023.129905.

Zhang, Y., Xiao, S., Ma, R., Zhang, Z., He, J., 2025. Beyond gas supersaturation: dissecting the secondary formation of methane hydrate. Fuel 381, 133310. https://doi.org/10.1016/j.fuel.2024.133310.

Zhang, Z.C., Wu, N.Y., Liu, C.L., Hao, X.L., Zhang, Y.C., Gao, K., Peng, B., Zheng, C., Tang, W., Guo, G.J., 2022. Molecular simulation studies on natural gas hydrates nucleation and growth: A review. China Geol. 5 (2), 330–344. https://doi.org/10.31035/cg2022017.

Zheng, X., Cheng, L., Liu, B., Ban, S., Chen, G., 2022. A molecular dynamic simulation on the memory effect of methane hydrate. J. Mol. Liq. 363, 119831. https://doi.org/10.1016/j.molliq.2022.119831.